

Structure and Dynamics of the Dilauroylphosphatidylethanolamine Lipid Bilayer[†]K. V. Damodaran,[‡] Kenneth M. Merz, Jr.,^{*,‡} and Bruce Paul Gaber[§]*Department of Chemistry, The Pennsylvania State University, University Park, Pennsylvania 16802, and Center of Bio/Molecular Science and Engineering, Naval Research Laboratory, Washington, D.C. 20375**Received February 3, 1992; Revised Manuscript Received May 22, 1992*

ABSTRACT: A 200-ps molecular dynamics (MD) simulation trajectory of a model dilauroylphosphatidylethanolamine (DLPE) bilayer in water at 315 K has been generated. Segmental order parameters, electron density profiles, and water pair distribution functions have been calculated. Comparison to experiment is made where possible. The dynamics of the system has been studied by analyzing the velocity autocorrelation functions (VAF) of both water and lipid atoms. Furthermore, the diffusive properties of water have been analyzed by computing the mean square displacement (MSD) and orientational correlation function (OCF) of water in two regions around the bilayer. The calculated order parameters show a behavior similar to the liquid crystalline phase of other bilayers, but the region around C1-C3 does not show the expected behavior. The electron density profile shows features that are characteristic of the liquid crystalline phase. The radial distribution functions suggest ordering of water near the charged head groups, which results in about 15 water molecules solvating each lipid molecule. We find from the VAF, MSD, and OCF calculation that the water molecules near the head groups of the lipid bilayer move more slowly than those further away. The VAF of the hydrocarbon chains have features of low-frequency motions that are probably cooperative nature in addition to the high-frequency motions associated with bond angle and torsional motions.

Obtaining a molecular level understanding of the structure, function, and dynamics of biomembranes has been and still is of great interest (Gennis, 1989; Lipowsky, 1991). Biomembranes are very complicated structures, but are composed mainly of a phospholipid bilayer and membrane proteins. Natural bilayers consist of various molecules (generally phospholipids) that are composed of a polar head group to which are attached hydrophobic alkyl chains. These molecules have the tendency to aggregate to form the classic lipid bilayer structure, which consists of two monolayers that have the alkyl portions abutted up against one another and the polar head groups exposed to the surrounding solvent. Lipids have rather complicated phase properties, but for the lipid bilayer structure we need consider only two phases. At low temperatures, these systems are in a gel phase (L_β) wherein the lipids are less mobile, more ordered, and closely packed. An important feature of this phase is the propensity of the hydrocarbon tails to adopt the all trans configuration over a less ordered mixture of trans, gauche, and kinked alkyl chains that is associated with the liquid crystalline phase (L_α). This latter phase occurs at higher temperatures and is generally the phase in which a bilayer adopts at physiological temperature. Thermal disorder and a larger area per lipid give rise to a greater quantity of 'gauche' kinks, whose concentration increases near the ends of the hydrocarbon tails. The water molecules near the head group form a hydration shell which plays a crucial role in maintaining the bilayer structure and is of special importance in the high-temperature phase, where the inter-lipid separation is considerably larger than in the low-temperature gel phase and the lipid-lipid interactions are weak.

Numerous experimental techniques have been applied to lipid bilayers in order to elucidate, at the molecular level, the

structure and dynamics of these unique molecular aggregations. X-ray crystallography of a number of lipids that form bilayers have given us insights into how these molecules pack against one another in an highly ordered environment. For example, dilauroylphosphatidylethanolamine (DLPE) (Elder et al., 1977; Hitchcock et al., 1974) and dimiristoylphosphatidylcholine (DMPC) (Pearson & Pascher, 1979) have had their crystal structures determined. These crystal structures provided insights into the molecular architecture of lipid bilayers. It appears that the lipid molecules in the crystal structures behave like lipids observed in a noncrystalline bilayer except for several important features. In the L_β or L_α forms gauche kinks are observed, and these phases have a larger area per lipid values. For example, the crystal structure of DLPE has a surface area per lipid of 39 Å², while L_β and L_α have areas per lipid of 41 and 50.6 Å², respectively (McIntosh & Simon, 1986a).

Insights into water penetration in a lipid bilayer come from neutron diffraction experiments. By taking the difference between structure factors obtained in D₂O and H₂O, the degree of water penetration can be estimated (Buldt et al., 1979; Zaccai et al., 1979). DLPE is known to adopt a lamellar structure, and McIntosh and Simon have used wide-angle X-ray diffraction studies on the hydrated lamellar phase (both L_β and L_α) of DLPE to show that a solvent layer of about 5 Å thickness exists between the bilayers (McIntosh & Simon, 1986a). The thickness of the fluid space between DLPE bilayers is rather small when compared to DMPC, for example (Rand, 1981). The thinness of the fluid space suggests that there is significant hydrogen bonding (through the intervening waters) between the opposing head groups or that there is potentially strong electrostatic interactions between the opposing amine and phosphate groups.

A very powerful technique to get both structural and dynamic information regarding the fatty acid chains comes from nuclear magnetic resonance (NMR). The quadrupole splitting measured in the ²H NMR of oriented bilayer samples

[†] We thank the Office of Naval Research for supporting this research (N00014-90-3-4002).

[‡] The Pennsylvania State University.

[§] Naval Research Laboratory.

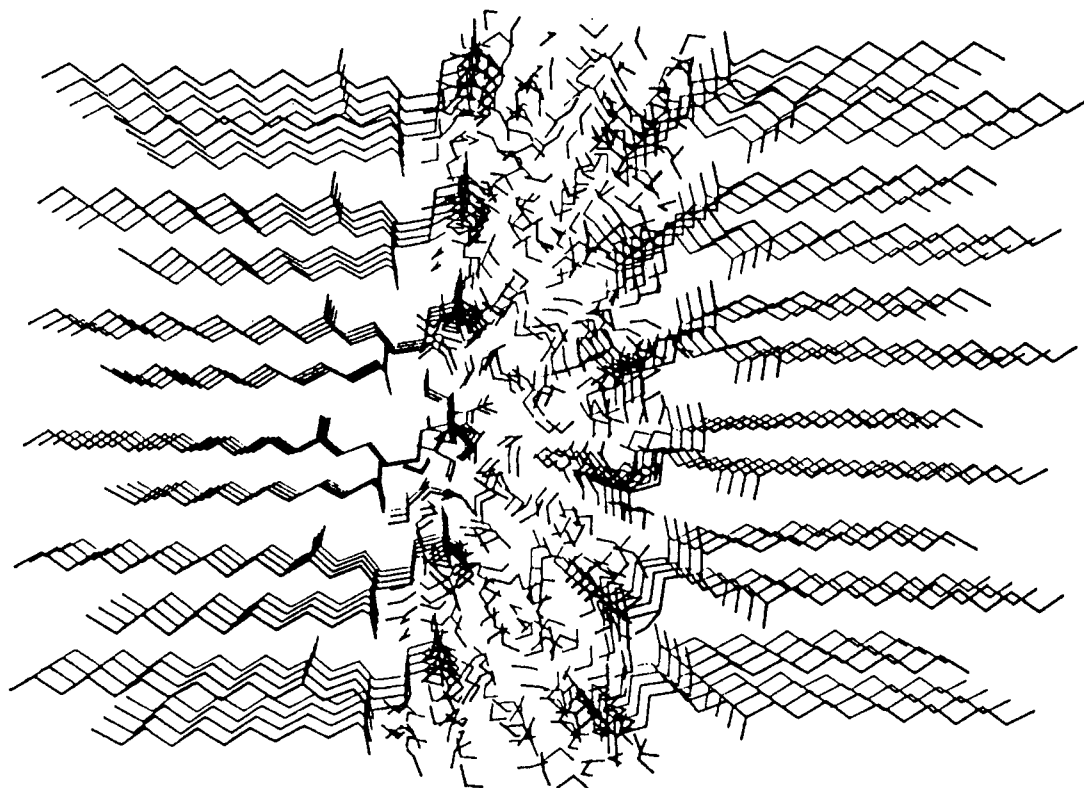


FIGURE 1: Starting configuration for the DLPE-water simulations. There are 48 lipid molecules and 553 water molecules. Dimensions of the simulation box: $X = 49.589$ Å, $Y = 35.560$ Å, and $Z = 34.140$ Å. X direction is along the bilayer normal.

depends on the orientation of the C–D plane with respect to the magnetic field and is used to define an order parameter for the carbon atoms on the hydrocarbon tails (Seelig, 1977; Seelig & Browning, 1978; Seelig & Seelig 1974; Boden et al., 1991; Davis, 1983). These studies give us insights into the number of gauche kinks present as we traverse down the fatty acid chain. Thus, the L_α phase is less ordered (i.e., more gauche kinks) than the L_β phase based on these measurements.

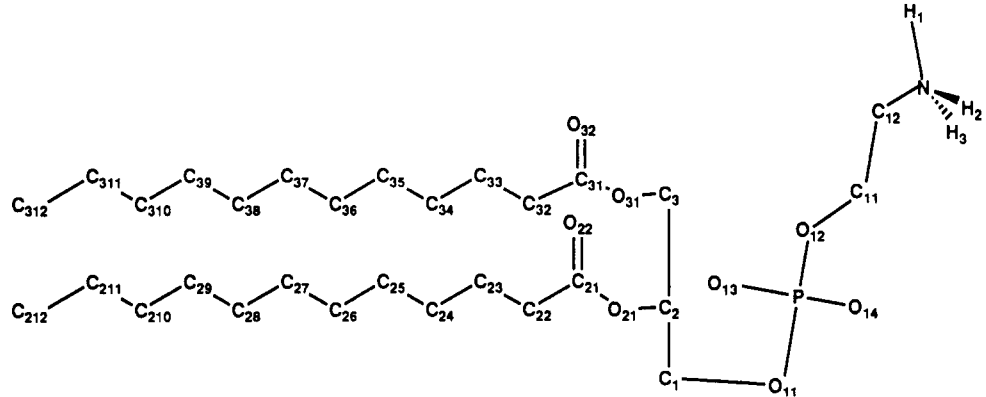
Modeling the structural and dynamical aspects of amphiphilic systems has been of great interest in recent years. However, the accurate modeling of these systems poses many problems. In particular, to realistically model these systems requires numerous amphiphilic molecules as well as counterions and water molecules. This necessarily results in a very large aggregate system when modeling at the all-atom or united-atom level. Furthermore, many of the interesting dynamical processes (e.g., phase transitions) occur over very long timescales. This coupled with the expense of carrying out all-atom simulations has led to the development of ingenious simplifications of the molecular and environmental representations (Smit et al., 1990; Gunn and Dawson 1989). Though, these models lack in atomic-level detail, they are very powerful techniques to model large aggregate systems and long time scale properties.

Regardless, of the success of the simple models, it is still of great interest to obtain molecular-level details regarding the structure and dynamics of amphiphilic systems. Recently, structure refinement and energy minimization studies have been performed on the DMPC and DLPE crystal structures by Vanderkooi (1991, 1990). The minimized lattice constants and cell volume are in good agreement with results from X-ray diffraction experiments (Elder et al., 1977; Hitchcock et al., 1974; Pearson & Pascher, 1979). Klein and co-workers have worked extensively using atom–atom potentials to describe the short time scale dynamics of amphiphilic systems (Watanabe & Klein, 1991, 1989). Computer simulation

techniques have been extensively used to study the structure of bilayer models also. Scott and co-workers have reported a number of Monte Carlo simulations aimed at understanding lipid–protein and lipid–cholesterol interactions (Scott, 1977, 1986, 1991; Scott & Cherng, 1978; Scott & Kalaskar, 1989). MD studies have been performed by van der Ploeg and Berendsen (1983, 1982) on decane bilayer models in the absence of explicit solvent. Subsequent work by Egberts and Berendsen (1988) on sodium decaonate/decanol system had water molecules included explicitly. Brownian dynamics (Pastor et al., 1988) and mean field stochastic boundary molecular dynamics (De Loof et al., 1991) simulations have been performed to investigate the NMR order parameter profile of DPPC. This type of calculation has the advantage that very long simulation times (several nanoseconds) can be achieved since the simulations are performed on a system of relatively small size. These simulations do not incorporate explicit solvent molecules nor do they consider “bulk” bilayer effects. To overcome this the force field used in these simulations incorporate both a stochastic term and a term that represents solvent–lipid and lipid–lipid interactions in an average way (Marcelja, 1973, 1974). A recent report, using a restrained bilayer model, has focused on the oscillatory behavior of the orientational polarization of water between DLPE bilayers (Berkowitz & Raghavan, 1991).

Our efforts have centered on developing a model of a lipid bilayer that gives a full representation of the water–lipid system. We feel that many of the simpler model systems described above are useful in many instances, but that a full accounting of the lipid–lipid and lipid–water interactions present in a bilayer will be required to garner a thorough understanding of the structure and dynamics of bilayers. In the present report we describe a 200-ps MD simulation of a liquid crystalline DLPE bilayer model with inclusion of explicit solvent.

Table I: STO-3G ESP Derived Atomic Point Charges for DLPE



atom	charge	atom	charge	atom	charge
N	-0.4183	C21	0.6482	O31	-0.4673
H1	0.3362	O22	-0.4374	C31	0.6407
H2	0.3362	C32	-0.0028	O32	-0.4267
H3	0.3362	C33	-0.0533	C22	-0.0198
C12	0.2946	C34	0.0486	C23	0.0055
C11	0.1162	C35	0.0129	C24	-0.0131
O12	-0.5247	C36	-0.0252	C25	0.0104
P	1.4799	C37	0.0070	C26	0.0091
O13	-0.7898	C38	0.0066	C27	-0.0065
O14	-0.7898	C39	-0.0089	C28	-0.0044
O11	-0.5247	C310	-0.0058	C29	0.0028
C1	0.1691	C311	0.0086	C210	0.0035
C2	0.1987	C312	-0.0102	C211	0.0086
O21	-0.4216	C3	0.2692	C212	-0.0098

COMPUTATIONAL DETAILS

The bilayer-water system was built from the crystal structure of DLPE (Elder et al., 1977; Hitchcock et al., 1974) by increasing the lipid-lipid separations proportionally so as to obtain the required surface area. The model consisted of 48 lipid molecules forming two monolayers with the head groups facing each other with a water slab of thickness ~ 5 Å (553 water molecules or ~ 11 waters per lipid) in between. Figure 1 gives the structure of the starting configuration used in our simulations. The calculations were performed using the AMBER 3.0 (Singh et al., 1986) MD program with periodic boundary conditions in all (x , y , and z) directions (see Figure 1). Through the use of periodic boundary conditions the model given in Figure 1 simulates a multilamellar lipid bilayer and not an isolated monolayer. Electrostatic interactions were modeled using partial charges obtained from *ab initio* quantum mechanical electrostatic potential fitting (ESP) calculations (B. H. Besler and K. M. Merz, Jr., unpublished results; Besler et al., 1990) using the GAUSSIAN 88 program at the STO-3G* level (Frisch et al., 1988). The bond, angle, and torsion parameters were taken directly from the AMBER force field (Weiner et al., 1984). These parameters have been found to be satisfactory in the force field development for crystalline lipid systems, from the minimization and dynamic simulations of crystalline 1- α -glycerylphosphorylcholine (GPC) and 2,3-dilaurylglycerol (DLG) (Stouch et al., 1991). The nonbonded interactions were modeled using OPLS parameters (Jorgensen & Triado-Rives, 1988) except for phosphorous for which the AMBER value itself was used. The 1-4 nonbonded and 1-4 electrostatic interactions were scaled by a factor of 8 and 2, respectively. This reproduces the torsional barriers (particularly those in the hydrocarbon chains) as it would using the default AMBER force field. Our torsion profile is very similar in shape to the widely used and accepted model for hydrocarbon torsions developed by Ryckaert and Bellemans (1975, 1978). All nonpolar groups (CH, CH₂, and CH₃) were treated as

united atoms. The partial charges used in the simulation are given in Table I. All bond lengths were constrained to their equilibrium values by the SHAKE procedure (Ryckaert et al., 1977). We have used the SPC/E water model (Berendsen et al., 1987) for the simulations. The water-water interactions in the system were minimized using the belly procedure (i.e., the lipids were held fixed and the water molecules around them were allowed to relax) prior to minimization of the whole system. This was followed by a 9-ps belly molecular dynamics simulation of the solvent only and then an equilibration phase of 41 ps. The calculations were performed at constant volume and constant temperature (Berendsen et al., 1984) of 315 K, well above the gel-liquid crystalline phase transition temperature (303.5 K) (Blume, 1983). A time step of 0.0015 ps and a nonbonded cutoff distance of 10 Å were used. We used a residue-based cutoff procedure, where each individual water and lipid molecule was considered as a residue. Following the 50-ps equilibration phase, a production run of 150 ps was carried out. The velocities and coordinates were saved every 10 time steps (every 0.015 ps), and the resulting trajectories were analyzed.

RESULTS AND DISCUSSION

A typical snapshot of the bilayer-water system along the MD trajectory is given in Figure 2. We have visualized the dynamics trajectories, and some of the interesting features that are readily apparent are as follows: (1) the lipid head groups remain largely parallel to the bilayer surface; however, a small fraction of them extend into the solvent or bend toward the hydrocarbon region due to intralipid and interlipid hydrogen bonding between the ammonium hydrogens and the nonesterified oxygens on the phosphate groups and (2) the presence of a significant amount of disorder in the fatty acid chain region which is characteristic of the liquid crystalline phase.

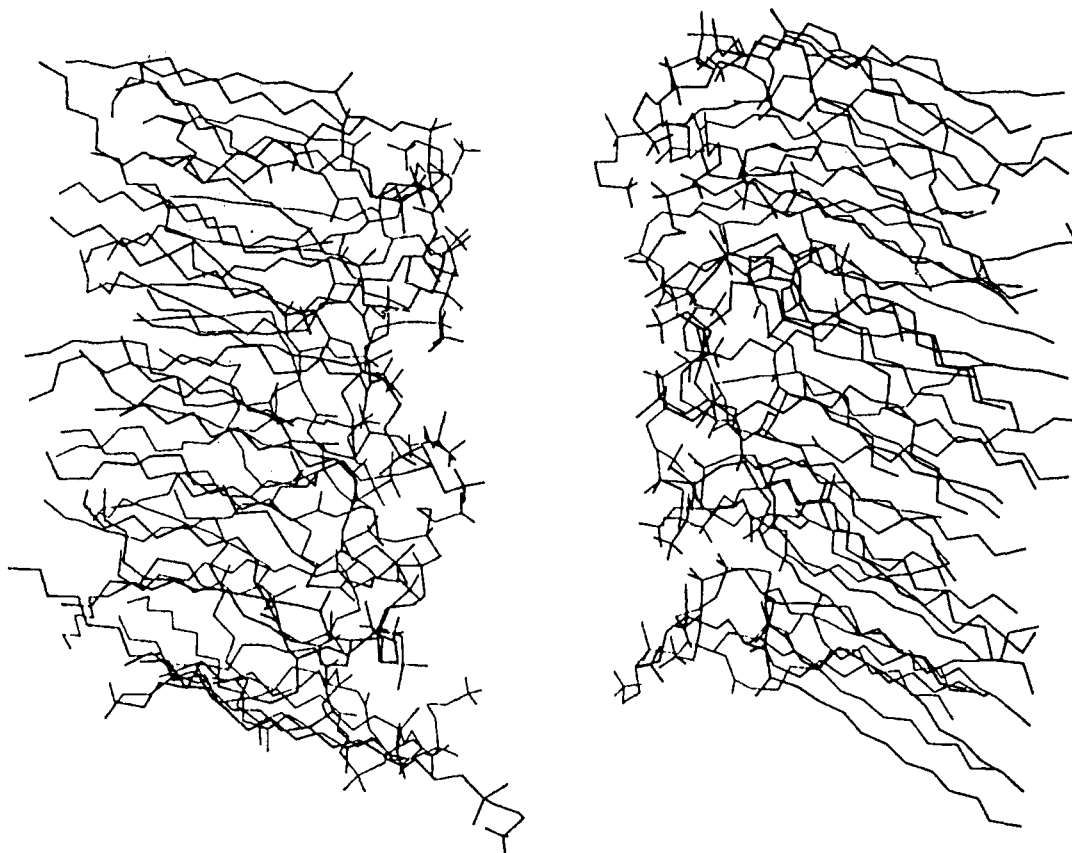


FIGURE 2: Typical snapshot of the DLPE-water system along the MD trajectory. The one given here is 90 ps after the equilibration phase. The solvent molecules are not shown for clarity.

In order to quantify the dynamics of the alkyl chains of the lipids, we have calculated order parameter profiles. The molecular long-axis order parameters were calculated as

$$S_j^{\text{mol}} = 1/2 \langle 3 \cos^2 \beta_j - 1 \rangle \quad (1)$$

where β_j is the angle between the bilayer normal and the long molecular axis (defined as the normal to the plane spanned by the two C-H vectors of the carbon atom j) of the hydrocarbon tail. As shown by Pastor et al. (1988), β is also equal to the angle between the bilayer normal and the vector joining the carbons $j-1$ and $j+1$. Since we have used united-atom carbons in our simulations, we have calculated the molecular long-axis order parameters using eq 1. This method requires the coordinates of carbons $(j-1)$ and $(j+1)$ for the evaluation of β_j ; therefore, the order parameter for the terminal carbon atom in the hydrocarbon chains cannot be calculated. The NMR order parameters are defined as

$$S_j^{\text{nmr}} = 1/2 \langle 3 \cos^2 \theta_j - 1 \rangle \quad (2)$$

where θ_j is the angle between the bilayer normal and the C-H vectors at the carbon atom j . Assuming an axially symmetric movement of the CH_2 segment about the long molecular axis, S_j^{nmr} can be obtained from S_j^{mol} as (Seelig, 1977)

$$S_j^{\text{nmr}} = -0.5 S_j^{\text{mol}} \quad (3)$$

In the all trans conformations S_j^{mol} will be unity, and in the isotropically disordered state, S_j^{mol} will be zero. The calculated order parameters are shown in Figure 3a.

We are unaware of an experimental order parameter profile for a liquid crystalline DLPE bilayer. Therefore, we cannot expect to exactly quantitate possible errors in our calculated order parameter profile. However, comparison with experimental order parameter profiles of other lipids is possible

(e.g., DPPC, DMPC, etc.) (Seelig & Seelig, 1974). Seelig and Browning (1978) have shown that the order parameter profiles of different lipids can be compared at the same reduced temperature $T_r = (T - T_c)/T_c$, where T_c is the gel to liquid crystalline phase-transition temperature. This eliminates the effects caused by the differences in the phase-transition temperatures. The present simulation has been done at $T_r = 0.0379$, in the reduced temperature scale. We have given in Figure 3a the order parameter profile for DPPC (1- α -dipalmitoylphosphatidylcholine) from ^2H -NMR measurements at $T_r = 0.0287$ by Seelig and Seelig (1974), for comparison. Overall the order parameter profile is quite reasonable. However, the magnitudes of the order parameters in our plot are a bit too high even when compared to the experimental profile at a lower reduced temperature, which suggests that our model is more ordered. A histogram of the dihedral angles in the hydrocarbon chains averaged over the MD trajectory show that about 73% of the dihedral angles are in the 160 – 180° range (see inset in Figure 3a), while the remainder adopt the gauche (30 – 90° range) conformation. Experimental order parameter profiles show a dip on going from the second to the third carbon atom, while our profile does not show this characteristic behavior. After the dip at carbon atom three, the profile usually increases and then drops off rapidly. Our profile also shows this behavior. The way in which we determined the order parameters does not allow us to obtain the order parameter for the terminal carbon, but we expect this to be in the range of 0.3 – 0.4 .

We have also shown in Figure 3a the individual contributions to the total order parameter profile from the sn-1 and sn-2 chains. These are very similar for both chains except at carbon positions 2 and 5. While the difference at carbon atom 2 may be due to the difference in the orientation of sn-1 and sn-2

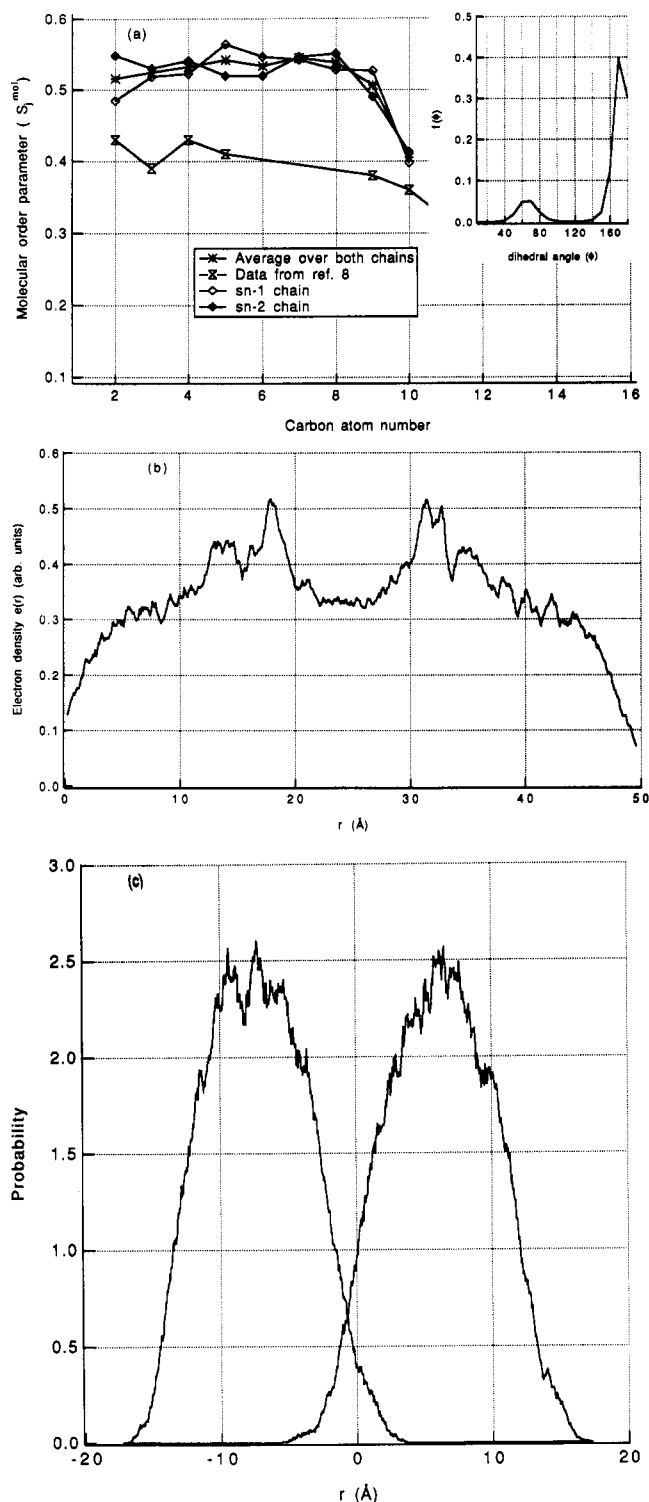


FIGURE 3: (a) Molecular order parameters (S_m^{mol}) averaged over the MD trajectory. The carbons C32 and C22 were numbered 1 in the sn-1 and sn-2 chains, respectively. The order parameters for these carbons and the terminal carbons (C312, C212) were not calculated. (See Table I for labeling.) The inset shows the average distribution of $-\text{CH}_2-\text{CH}_2-$ torsions. (b) Calculated electron density distribution along the bilayer normal. (c) Probability distribution of alkyl carbon atoms along the bilayer normal.

chains, the reason for the difference at carbon atom 5 is not clear.

The electron density profile $[e(r)]$ of the bilayer–water model is given in Figure 3b. This was evaluated by sampling over the full production phase of the simulation (150 ps). The maxima at 18 and 31 Å correspond to the polar head group region, while the hydrocarbon tails give rise to the low-electron

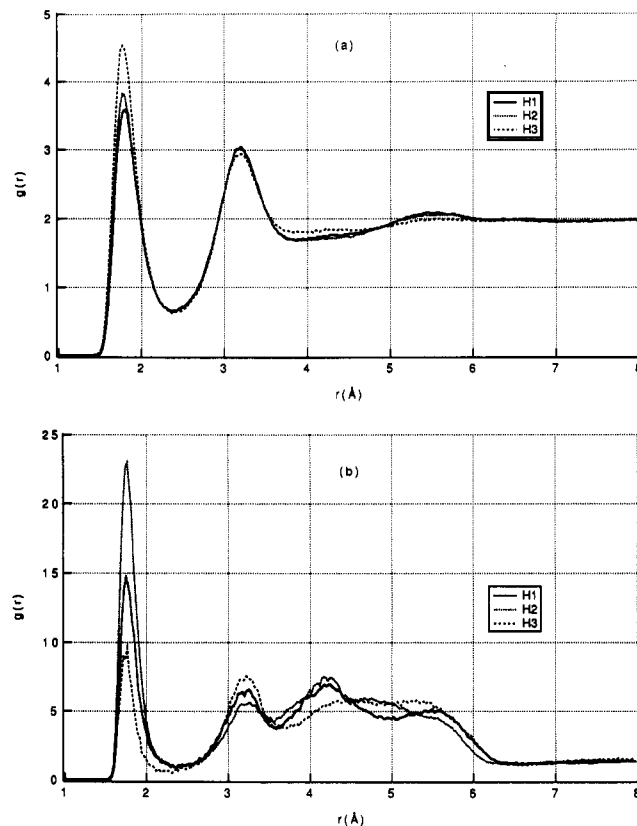


FIGURE 4: (a) Radial distribution functions of water with respect to the three ammonium hydrogens (H1, H2, and H3) of the DLPE head group. (b) Radial distribution functions of the nonesterified oxygens O13 and O14 of the phosphate group with respect to the ammonium hydrogens H1, H2, and H3. Both intralipid and interlipid contributions are included.

densities in the outer region. The low-electron density region between the polar head groups represents the aqueous environment. The variation of electron density along the bilayer normal has features characteristic of the liquid crystalline phase (McIntosh & Simon, 1986a).

The distribution of the alkyl chain carbon atoms along the bilayer normal is given in Figure 3c. This figure very nicely shows the degree of intercalation between the two monolayers that constitute a bilayer. The intercalation of the alkyl chains from one DLPE monolayer into another is about 4 Å in from the bilayer center. This distance seems reasonable and indicates that over the time scale of our simulation the bilayer is not coming apart. However, there is no experimental data clearly indicating the depth to which one monolayer will penetrate into another.

The aqueous environment of the lipid head group atoms was probed by calculating the radial distribution functions $[g(r)]$ which were obtained as

$$g(r) = N(r)/(4\pi r^2 \rho_0) \quad (4)$$

where $N(r)$ is the number of water molecules between r and $r + \delta r$ from the reference atom. ρ_0 is the bulk water number density (taken as the number of water molecules per volume of the computational box). Since we consider the large volume occupied by lipids also, this gives a lower value for ρ_0 , hence the $g(r)$ s are higher than 1.0 at large distances instead of 1.0 as in typical $g(r)$ plots.

The calculated $g(r)$ s are given in Figures 4–6. The presence of hydrogen bonding between the ammonium hydrogens and the water oxygens give rise to the sharp peak at 1.80 Å in Figure 4a. The area under this peak suggests a coordination

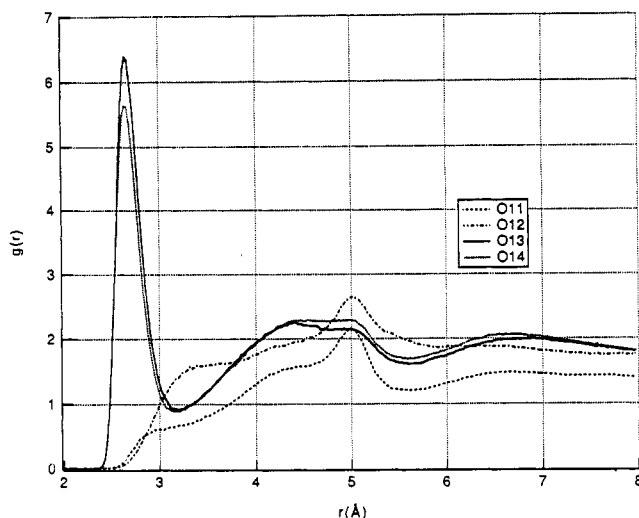


FIGURE 5: Radial distribution functions of water with respect to the oxygens of the phosphate group.

number of ~ 0.65 . Summing over all of the ammonium $\text{H} - \text{O}(\text{wat}) g(r)$ s gives a total coordination number of ~ 2.03 . The second coordination shell of the three ammonium hydrogens overlap, and the coordination number at 4 Å is estimated to be ~ 4.4 waters per each ammonium hydrogen. In addition to hydrogen bonding to water, the ammonium hydrogens participate in intra/interlipid hydrogen bonding (within a monolayer) with the nonesterified oxygens of the phosphate groups O13 and O14. The pair distribution functions of these interactions are shown in Figure 4b. This plot shows significant structure and indicates that there are strong contacts between the ammonium hydrogens and the nonesterified phosphate oxygens. Chemically the three hydrogens H1, H2, and H3 are expected to be equivalent when they are averaged over time. Similarly the two oxygens O13 and O14 can be considered as being equivalent over long timescales. However, the finite length of the simulation does not allow for adequate sampling of $\text{N}(\text{H})_3 - \text{O}(\text{wat})$ and $\text{N}(\text{H})_3 - \text{O}-\text{P}$ distances. This gives rise to unequal intensities in the first peak of the $g(r)$ plots given in Figure 4. This argument is further verified by examining the complementarity of the first peak intensities in Figure 4a and b. For example, H3 which has the highest $\text{O}(\text{wat})$ first peak coordination number in Figure 4a has the lowest (O13,O14) first peak and coordination number in Figure 4b. The remaining ammonium hydrogens do not follow this trend exactly, but still do indicate that the sampling is not complete at the time scales we have employed.

The $\text{P}-\text{O} - \text{O}(\text{wat})$ pair distribution functions are given in Figure 5. The esterified oxygens O11 and O12 do not appear to have well-defined hydration shells. The water pair distribution functions of O13 and O14 show a strong solvation shell in contrast to the esterified oxygens. From Figures 4b and 5 we conclude that O13 and O14 are hydrogen bound to both the ammonium hydrogens and water molecules, while the esterified oxygens appear not to be involved in any strongly structured hydrogen bonding. This is not surprising given our charge model, which places a much smaller charge on the esterified oxygens than on the nonesterified ones (-0.52 versus -0.79). The $\text{P} - \text{O}(\text{wat}) g(r)$ given in Figure 6a has a maximum at 3.825 Å and shows a clear hydration shell of about 5 water molecules out to the first minimum at approximately 4.5 Å. The waters hydrogen bonded to the ammonium hydrogens make the main contribution to the first peak at 2.75 Å in the $\text{N} - \text{O}(\text{wat}) g(r)$ given in Figure 6b.

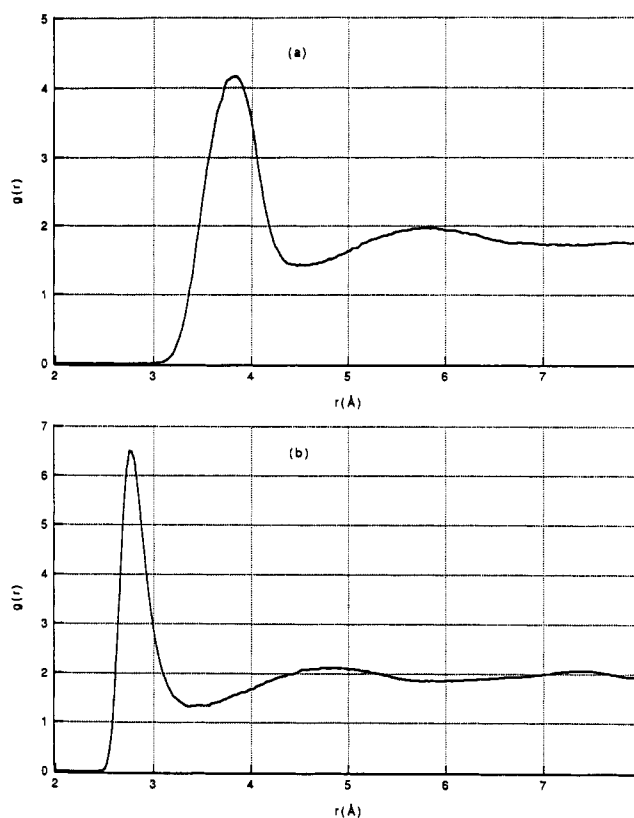


FIGURE 6: Radial distribution functions of water with respect to (a) phosphorous and (b) nitrogen of the DLPE head group.

There are 2.5 waters in the first hydration shell at the first minimum at about 3.5 Å, and there are about 15 water molecules at the second minimum at approximately 6.0 Å. The summation of the water molecules up to the first minimum in Figure 4a (2.03 waters) is in reasonable agreement with that found in the first minimum in Figure 6b (~ 2.5 waters).

McIntosh and Simon (1986a) have estimated from diffraction and dilatometry measurements that fully hydrated DLPE has ~ 10 waters per lipid in the liquid crystalline phase. ^2H -NMR of hydrated phosphatidylethanolamine (Borle & Seelig, 1983) shows the presence of a primary hydration shell of 11–16 waters per lipid in rapid exchange with bulk water. To make an estimate of the number of water molecules associated with a lipid, we can consider the first coordination shell of the ammonium ions (see Figure 4a), which gives a value that is too low (2.03). However, considering fact that the ammonium hydrogens have a clear second coordination shell, we can take the total the coordination number at 4 Å; we get ~ 13 water molecules. A similar estimate can be made from the minimum at 6 Å in the $\text{N} - \text{O}(\text{wat}) g(r)$ (see Figure 6b), which suggests a hydration shell of ~ 15 water molecules. An important feature to note is that these hydration shells overlap with those of other lipids in the bilayer. This, therefore, makes it difficult to obtain a number that is indicative of how many water molecules are clearly associated with any one lipid.

In order to study further the dynamics of the system, we have calculated the velocity autocorrelation function (VAF) and the mean square displacement (MSD) of water molecules. All waters within 4 Å from any lipid ammonium hydrogen were treated as bound waters, and those beyond 4 Å from all lipid ammonium hydrogens were treated as bulk waters. A distance of 4 Å was chosen as the boundary for bound waters since the second coordination shell for the ammonium hydrogens extends up to 4 Å (see Figure 4a). However, the

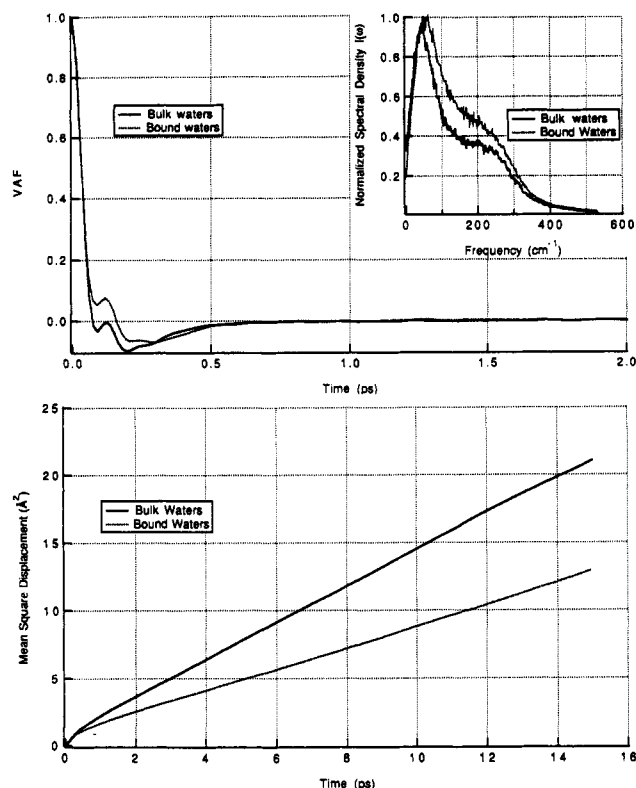


FIGURE 7: (a) Velocity autocorrelation functions (VAF) and (b) mean square displacement (MSD) plots of the solvent water molecules. (See text for the description of bound and bulk waters.) Inset in (a) shows the normalized spectral density obtained from the VAFs.

bound/bulk nature of a given water molecule was determined only after evaluating its distance from any head group atom (i.e., from the ester carbonyls on up) of any lipid molecule. Thus, bulk waters are beyond 4 Å from all lipid head group atoms and bound are within 4 Å of any head group atom. On average, there were 160 bulk waters out of the 553 waters solvating the lipids. Since there could be exchange between bound and bulk waters, the status of each water molecule was updated every picosecond. More frequent updates had little effect on the results. VAFs were calculated as

$$c(t) = \langle v(0)v(t) \rangle / \langle v(0)v(0) \rangle \quad (5)$$

and the spectral density function $I(\omega)$ was obtained as

$$I(\omega) = \int_0^{t_{\max}} c(t) \cos(\omega t) dt \quad (6)$$

and the mean square displacements were obtained as

$$\text{MSD}(t) = \langle |r(t) - r(0)|^2 \rangle \quad (7)$$

The angular brackets in eqs 5 and 7 imply averaging over the entire MD trajectory. The velocities and coordinates refer to those of the centers of mass of the water molecules. The MSD and VAF calculations do not take into full account the migration of a water molecule between an initial time 0 and a final time t (see eq 5), which may cause some artifacts in these calculations at the longer time scales. However, we expect this error to be small, especially in the important short time region (i.e., from 0 to 1 ps). The velocity autocorrelation function and the normalized spectral density function of bound and bulk water molecules are given in Figure 7a. $I(\omega)$ of bound waters show higher intensities in the high-frequency region. This suggests, not unexpectedly, that the bound waters are less free to move than are the bulk waters. However, the differences between the bound and bulk waters are not great,

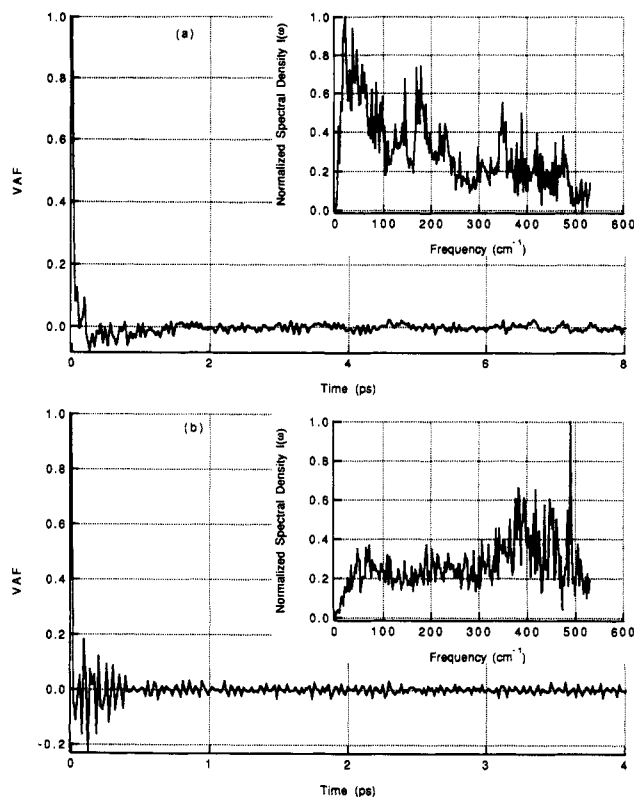


FIGURE 8: VAFs of (a) the lipid hydrocarbon tails and (b) the polar head groups. Note the difference in the time axis in Figure 7a and panels (a) and (b) of this figure adopted to clearly bring out the short time behavior of the VAFs. The corresponding normalized spectral density functions are shown as insets.

which suggests that the exchange between the bound and bulk state is relatively facile.

The mean square displacement plots given in Figure 7b clearly differentiate between the bulk and bound waters. The data of Figure 7b suggest that the bound waters diffuse at a slower rate than do the bulk waters. The calculated diffusion constants for the bulk waters ($2.4 \times 10^{-5} \text{ cm}^2 \text{ s}^{-1}$) are in good agreement with the reported value of $2.5 \times 10^{-5} \text{ cm}^2 \text{ s}^{-1}$ for SPC/E water (Berendsen et al., 1987), and a test MD simulation of neat water using our programs gave a diffusion constant of $2.59 \times 10^{-5} \text{ cm}^2 \text{ s}^{-1}$, which is also in good agreement with the previously reported value. The bound waters have a calculated diffusion constant of $1.34 \times 10^{-5} \text{ cm}^2 \text{ s}^{-1}$, which is about a factor of 2 less than that for bulk waters. This observation is in agreement with the VAF data described above in that it also suggests that the bound waters are less free to move than are the bulk waters.

VAFs were calculated for the hydrocarbon tails and the head group atoms separately and are presented along with corresponding spectral density plots in Figure 8a and b, respectively. Unlike those of solvent molecules, the VAFs have noticeable intensities even at 15 ps and have "fast" oscillations, presumably from bond angle and dihedral motions. The VAF of hydrocarbon tails has slow oscillations also due to collective motions, which may be the origin of the peak below 100 cm^{-1} in the power spectrum. The head groups are also expected to have collective motions, but the power spectrum is shifted relative to that seen for the hydrocarbon tails with the first large peak being in the 400-cm^{-1} range instead of 100 cm^{-1} . One interpretation of this data is that the head group region's collective motions appear at higher frequencies because of strong interlipid interactions that restrict the motion of the head groups. This restriction would

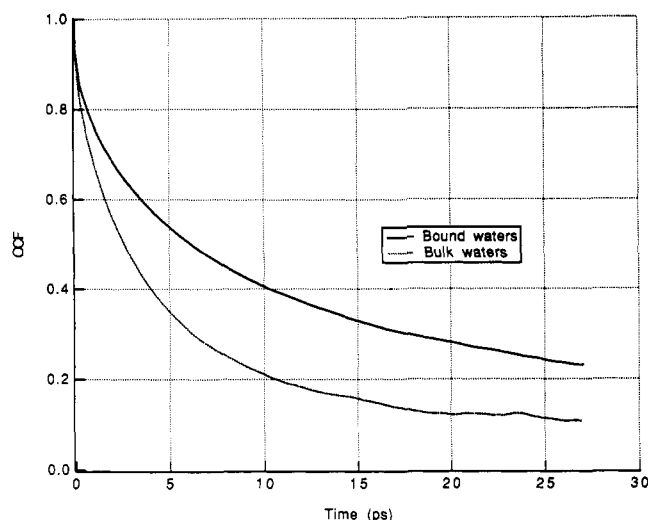


FIGURE 9: Orientational correlation function (OCF) of the solvent molecules.

come from the previously described interlipid hydrogen bonds between the ammonium hydrogens on one lipid and the phosphate oxygens on another lipid. This would result in a stronger interlipid interaction (from hydrogen bonding) than that present in the hydrocarbon tail region (hydrophobic contacts only). Hence, we can view the head group region as being more tightly associated and less fluxional than the hydrocarbon tail region.

As a final probe of the water dynamics we have calculated the orientational correlation function (OCF) using the following expression:

$$c(t) = \langle \mathbf{u}(0)\mathbf{u}(t) \rangle / \langle \mathbf{u}(0)\mathbf{u}(0) \rangle \quad (8)$$

where $\mathbf{u}(t)$ is the C2 axis of the water molecule. Figure 9 gives the OCF for the bound and bulk waters using the same definition as given above. The OCF of the bulk waters decays much more rapidly than does the OCF for the bound waters, which is again indicative of a strong interaction between the head groups of the lipids and the "bound" water molecules.

CONCLUSIONS

We have presented results from a 200-ps molecular dynamics simulation of a DLPE lipid bilayer. The simulation has been successful in reproducing several features of bilayer dynamics and indicates that in the future MD of bilayer systems will be a very fruitful research area because of the ability of this method to provide molecular-level insights into the structure, function, and dynamics of these systems. The present simulation is of a fairly short duration and as such is most useful for examining short time scale motions (gauche kinking, water dynamics, etc.) (Gennis, 1989). In order to study longer time scale, motions (lipid diffusion, lipid flip-flopping, etc.) will clearly require simulations of significantly longer time scales (ns, μ s, or even ms) (Gennis, 1989; Pastor et al., 1991). These phenomenon will certainly be studied in the future.

Our MD simulation reproduces the order parameter profile for the DLPE bilayer reasonably well and suggests that 27% of the torsions are in the gauche conformation and 73% are in the trans conformation. However, we find that the characteristic dip present in experimental order parameter profiles at the C2 position is missing. This may be due to the time scale of our simulation, but we have examined this possibility and find that the order parameter profile rapidly converges at about 50–100 ps and does not change between 100 and 150 ps. Hence, it is likely that the problem in our

order parameter profiles has more to do with errors in the molecular mechanical potential than any other error source. How exactly to improve the behavior at the C2 position is not clear, but certainly alternative torsion parameters may be necessary. However, the parameters utilized here are quite reasonable overall and give order parameters that are in good accord with the experimental values. Other workers have evaluated order parameter profiles using various simulation methods and obtain results either slightly better or similar to ours (Scott & Kalaskar, 1989; DeLoof, 1991; Egberts & Berendsen, 1988; Pastor et al., 1988, 1991).

The electron density profile from our MD simulation has features that are characteristic of the liquid crystalline phase of the DLPE bilayer. It is encouraging that we are able to reproduce this information; however, the electron density profile is not a sensitive indicator of bilayer structural disorder as, for example, is the order parameter profile. It does, however, suggest that our charge model is reasonable.

The $g(r)$ plots have revealed several interesting features of the dynamics of the DLPE bilayer. First, we find that there are reasonably strong hydrogen bonds between the ammonium hydrogens on one lipid with the nonesterified oxygens on an adjacent lipid. These interactions rigidify the head group region of the bilayer by in essence "cross-linking" the lipid head groups together. Secondly, there are strong hydration shells around the ammonium hydrogens and the nonesterified oxygens in the head groups region of the lipid, which leads to about 15 water molecules surrounding each lipid molecule. The hydration shells of adjacent lipids overlap with one another, and as a result several of the 15 water molecules surrounding one lipid will be shared with an adjacent one. It will be interesting to probe the bound waters for their orientational order, particularly in the case of choline head groups (e.g., DMPC) where the thickness of the intermediate water layer is much larger than in DLPE. Correlation of the present information with data obtained on a DMPC bilayer (K. V. Damodaran and K. M. Merz, Jr., Manuscript in preparation) will provide insights into the so-called hydration force problem (McIntosh & Simon, 1986b; Rand & Parsegian, 1989; Israelachvili & Wennerstrom, 1992).

The velocity autocorrelation function and spectral density function of the bound and bulk classes of waters show the expected behavior. The bound waters are found to be shifted into the higher frequency region of the power spectrum, which indicates that they are more constricted in their movements than are the bulk waters. This observation is borne out in the mean square displacement plot and in the orientational correlation plot, which both indicate that the bound waters diffuse more slowly and reorient themselves more slowly than do bulk waters. Comparison of the water diffusion behavior in a DLPE-based bilayer with that for a DMPC one will be very interesting and will provide insights into the hydration force problem (McIntosh & Simon, 1986b; Rand & Parsegian, 1989; Israelachvili & Wennerstrom, 1992). At this point we can say that water molecules at the lipid–water interface in a DLPE-based bilayer are not as mobile as water molecules further out. Furthermore, the hydration force is thought to arise from the energetic expense of removing waters of hydration. Hence, this leads us to the supposition that the DMPC-based bilayer might exhibit this same behavior to a greater extent. However, the molecular-level details of how this phenomenon occurs may be different in the two cases. For the head group region and the alkyl tail region of the bilayer, we find that the latter region is more fluxional than the former and that this is probably due to reasonably strong

interlipid hydrogen bond interactions between the ammonium hydrogens and the nonesterified phosphate oxygens.

The simulation reported here has been reasonably successful in reproducing the expected features of the short time scale dynamics of a DLPE-based lipid layer. Various aspects of the interfacial dynamics of the water molecules and the water penetration into the lipid bilayer have been identified. The dynamics of the alkyl chains are well represented except for the C1–C3 region of the order parameter profile. Future work will certainly focus on correcting this weakness. However, the model we have used is quite reasonable and indicates that MD simulations will be an ever more powerful tool in the study of the structure, function, and dynamics of lipid bilayers and their interactions with other molecules.

ACKNOWLEDGMENT

We thank S. Simon and O. Andersen for helpful discussions. We thank the Pittsburgh Supercomputer Center for Cray YMP time.

REFERENCES

- Berendsen, H. J. C., Postma, J. P. M., van Gunsteren, W. F., DiNola, A. D., & Haak, J. R. (1984) *J. Chem. Phys.* **81**, 3684.
- Berendsen, H. J. C., Grigera, J. R., & Straatsma, T. P. (1987) *J. Phys. Chem.* **91**, 6269.
- Berkowitz, M. L., & Raghavan, K. (1991) *Langmuir* **7**, 1042.
- Besler, B. H., Merz, K. M., Jr., & Kollman, P. A. (1990) *J. Comput. Chem.* **11**, 431.
- Blume, A. (1983) *Biochemistry* **22**, 5436.
- Boden, N., Jones, S. A., & Sixl, F. (1991) *Biochemistry* **30**, 2146.
- Borle, F., & Seelig, J. (1983) *Biochim. Biophys. Acta* **735**, 131.
- Buldt, G., Gally, H. U., Seelig, J., & Zaccai, G. (1979) *J. Mol. Biol.* **134**, 673.
- Davis, J. H. (1983) *Biochim. Biophys. Acta*, **737**, 117.
- De Loof, H., Harvey, S. C., Segrest, J. P., & Pastor, R. W. (1991) *Biochemistry* **30**, 2099.
- Egberts, E., & Berendsen, H. J. C. (1988) *J. Chem. Phys.* **89**, 3718.
- Elder, M., Hitchcock, P., Mason, R., & Shipley, G. G. (1977) *Proc. R. Soc. London* **354A**, 157.
- Frisch, M. J., Head-Gordon, M., Schlegel, H. B., Raghavachari, K., Binkley, J. S., Gonzalez, C., Defrees, D. J., Fox, D. J., Whiteside, R. A., Seeger, R., Melius, C. F., Baker, J., Martin, R. L., Kahn, L. R., Stewart, J. J. P., Fluder, E. M., Topiol, S., & Pople, J. A. (1988) GAUSSIAN 88, Gaussian, Inc., Pittsburgh, PA.
- Gennis, R. B. (1989) *Biomembranes: Molecular Structure and Function*, Springer-Verlag, New York.
- Gunn, J. R., & Dawson, K. A. (1989) *J. Chem. Phys.* **91**, 6393.
- Hitchcock, P. B., Mason, R., Thomas, K. M., & Shipley, G. G. (1974) *Proc. Natl. Acad. Sci. U.S.A.* **71**, 3036.
- Israelachvili, J. N., & Wennerstrom, H. (1992) *J. Phys. Chem.* **96**, 520.
- Jorgensen, W. L., & Triado-Rives, J. (1988) *J. Am. Chem. Soc.* **110**, 1657.
- Lipowsky, R. (1991) *Nature* **349**, 475.
- Marcelja, S. (1973) *Nature* **241**, 451.
- Marcelja, S. (1974) *Biochim. Biophys. Acta* **367**, 165.
- McIntosh, T. J., & Simon, S. A. (1986a) *Biochemistry* **25**, 4948.
- McIntosh, T. J., & Simon, S. A. (1986b) *Biochemistry* **25**, 4058.
- Pastor, R. W., Venable, R. M., & Karplus, M. (1988) *J. Chem. Phys.* **89**, 1112.
- Pastor, R. W., Venable, R. M., & Karplus, M. (1991) *Proc. Natl. Acad. Sci. U.S.A.* **88**, 892.
- Pearson, R. H., & Pascher, I. (1979) *Nature* **281**, 499.
- Rand, R. P. (1981) *Annu. Rev. Biophys. Bioeng.* **10**, 277.
- Rand, R. P., & Parsegian, B. A. (1989) *Biochim. Biophys. Acta* **988**, 350.
- Ryckaert, J. P., & Bellemans, A. (1975) *Chem. Phys. Lett.* **30**, 123.
- Ryckaert, J. P., & Bellemans, A. (1978) *Faraday Discuss. Chem. Soc.* **66**, 95.
- Ryckaert, J. P., Ciccotti, G., & Berendsen, H. J. C. (1977) *J. Comput. Phys.* **23**, 327.
- Scott, H. L. (1977) *Biochim. Biophys. Acta* **469**, 264.
- Scott, H. L. (1986) *Biochemistry* **25**, 6122.
- Scott, H. L. (1991) *Biophys. J.* **59**, 445.
- Scott, H. L., & Cherng, S.-L. (1978) *Biochim. Biophys. Acta* **510**, 209.
- Scott, H. L., & Kalaskar, S. (1989) *Biochemistry* **28**, 3687.
- Seelig, A., & Seelig, J. (1974) *Biochemistry* **13**, 4839.
- Seelig, J. (1977) *Q. Rev. Biophys.* **10**, 353.
- Seelig, J., & Browning, J. L. (1978) *FEBS Lett.* **92**, 41.
- Singh, U. C., Weiner, P. K., Caldwell, J. W., & Kollman, P. A. (1986) AMBER (UCSF), version 3.0.
- Smit, B., Hilbers, P. A. J., Esselink, K., Rupert, L. A. M., van Os, N. M., & Schlijper, A. G. (1990) *Nature* **348**, 624.
- Stouch, T. R., Ward, K. B., Altier, A., & Hagler, A. T. (1991) *J. Comput. Chem.* **12**, 1033.
- Vanderkooi, G. (1990) *J. Phys. Chem.* **94**, 4366.
- Vanderkooi, G. (1991) *Biochemistry* **30**, 10760.
- van der Ploeg, P., & Berendsen, H. J. C. (1982) *J. Chem. Phys.* **76**, 3271.
- van der Ploeg, P., & Berendsen, H. J. C. (1983) *Mol. Phys.* **49**, 233.
- Watanabe, K., & Klein, M. L. (1989) *J. Chem. Phys.* **93**, 6897.
- Watanabe, K., & Klein, M. L. (1991) *J. Phys. Chem.* **95**, 4158.
- Weiner, S. J., Kollman, P. K., Case, D. A., Singh, U. C., Ghio, C., Alagona, G., Profeta, S., & Weiner, P. (1984) *J. Am. Chem. Soc.* **106**, 765.
- Zaccai, G., Buldt, G., Seelig, A., & Seelig, J. (1979) *J. Mol. Biol.* **134**, 693.

Registry No. DLPE, 42436-56-6.